

Corrosion Behavior of HVOF-Sprayed Fe-Based Alloy Coating in Various Solutions

Lei Qiao, Yuping Wu, Sheng Hong, Yujiao Qin, Wei Shi, and Gaiye Li

(Submitted January 29, 2016; in revised form October 31, 2016; published online August 4, 2017)

A Fe-based amorphous/nanocrystalline coating was prepared by the high-velocity oxygen fuel (HVOF) spraying process. The coating was characterized by x-ray diffraction, scanning electron microscopy and transmission electron microscopy. The corrosion resistances of the Fe-based coating and a reference electroplated hard chromium (EHC) coating were evaluated in a 3.5% NaCl solution, a 1 mol/L HCl solution and a 1 mol/L NaOH solution using potentiodynamic polarization and electrochemical impedance spectroscopy (EIS). All of the results indicated that the corrosion resistance of the Fe-based coating was superior to the resistance of the EHC coating in both the 3.5% NaCl solution and the 1 mol/L HCl solution due to the dense structure and fewer defects of the Fe-based coating. However, the corrosion resistance of the Fe-based coating was inferior to corrosion resistance of the EHC coating in the 1 mol/L NaOH solution. This could be ascribed to the drastic passivation of the EHC coating in an alkaline environment.

Keywords corrosion resistance, Fe-based amorphous/nanocrystalline, HVOF spraying

1. Introduction

Due to their homogeneous composition and few crystal defects, amorphous coatings usually have both excellent mechanical properties and superior chemical performance. The lack of grains and grain boundaries results in their remarkable anti-corrosion properties (Ref 1-3). Among the various amorphous coatings, Fe-based amorphous coatings are well known for the combination of excellent corrosion behavior, outstanding wear resistance and relatively low cost (Ref 4-6). Due to these advantages, Fe-based amorphous coatings have shown promise for protecting engineering components from corrosion.

Electric arc spraying (Ref 7, 8), plasma spraying (Ref 9) and high-velocity oxygen fuel (HVOF) spraying (Ref 10, 11) are common technologies for preparing coatings, among which the HVOF spraying technology is considered to be one of the most competitive thermal spray processes to prepare high-quality coatings. During the HVOF spraying process, the feedstock particles are injected into a high-velocity hot gas jet generated through the combustion of oxygen and a fuel gas such as kerosene. Due to the extremely high velocity (approximately

700 m/s) and moderate temperature (approximately 2800 °C) of the in-flight particles obtained from the hot gas, coatings produced by HVOF always are denser, less oxidized and have a much better bonding condition than other methods such as plasma spraying (Ref 12). Equally important, these molten or half-molten particles are deposited on the substrate and cooled at a rate of approximately 10^4 K/s, which is fast enough to deposit many alloy compositions above their respective critical cooling rate to produce amorphous alloys. Therefore, HVOF is a good way to prepare amorphous coatings with a dense structure, outstanding adhesion and low oxidation.

Zhou et al. (Ref 13) and Zhang et al. (Ref 14) studied the corrosion behavior of an $\text{Fe}_{48}\text{Cr}_{15}\text{Mo}_{14}\text{C}_{15}\text{B}_6\text{Y}_2$ amorphous coating prepared by HVOF thermal spraying technology. They noted that this coating has an excellent ability to resist localized corrosion, and the corrosion resistance can be improved by optimizing spray parameters, including the kerosene flow and the oxygen flow. The improvement in the corrosion behavior of the coating was attributed to obtaining the proper proportion of porosity and amorphous fraction. Yang et al. (Ref 15) also reported that the corrosion resistance of an $\text{Fe}_{48}\text{Cr}_{15}\text{Mo}_{14}\text{C}_{15}\text{B}_6\text{Y}_2$ coating prepared by HVOF deteriorated with the increasing fraction of crystalline phases and that the corrosion pits always initiated at the boundaries around the crystalline phases. Liu et al. (Ref 16) prepared $\text{Fe}_{54.2}\text{Cr}_{18.3}\text{Mo}_{13.7}\text{Mn}_{2.0}\text{W}_{6.0}\text{B}_{3.3}\text{C}_{1.1}\text{Si}_{1.4}$ amorphous/nanocrystalline metallic coatings, and they found that these Fe-based coatings have an excellent erosion-corrosion resistance even in aggressive media. Bakare et al. (Ref 17) prepared an $\text{Fe}_{43}\text{Cr}_{16}\text{Mo}_{16}\text{C}_{15}\text{B}_{10}$ alloy coating by HVOF spraying technology and noted that the amorphous form of the coating shows better corrosion resistance than the crystalline form in both 0.5 mol/L H_2SO_4 and 3.5% NaCl electrolytes. This was attributed to the homogeneity of the amorphous coating and particularly to the elimination of the M₂₃C₆ phase that underwent preferential corrosion in the crystalline form of the material. Thus far, although some studies of Fe-based amorphous coatings have been conducted, research regarding the corrosion behavior and corrosion mechanism of Fe-based amorphous coatings in various solutions is still needed, especially in alkaline solution.

Lei Qiao, Yujiao Qin, Wei Shi, and Gaiye Li, College of Mechanics and Materials, Hohai University, 8 Focheng West Road, Nanjing 211100, People's Republic of China; Yuping Wu, College of Mechanics and Materials, Hohai University, 8 Focheng West Road, Nanjing 211100, People's Republic of China and Key Laboratory of Nuclear Materials and Safety Assessment, Institute of Metal Research, Chinese Academy of Sciences, 62 Wencui Road, Shenyang 110016, People's Republic of China; and Sheng Hong, College of Mechanics and Materials, Hohai University, 8 Focheng West Road, Nanjing 211100, Peoples Republic of China and Material Corrosion and Protection Key Laboratory of Sichuan Province, 180 Xueyuan Street, Zigong 643000, People's Republic of China. Contact e-mail: wuyuping@hhu.edu.cn.

In this work, HVOF spraying technology has been employed to prepare Fe-based amorphous/nanocrystalline coatings. The corrosion resistance of the Fe-based coating in a 3.5% NaCl solution, a 1 mol/L HCl solution and a 1 mol/L NaOH solution was presented and compared to the reference EHC coating.

2. Experiment

2.1 Preparation of the Coating

A commercially available Fe-based alloy powder manufactured by Solomon Technology was used in this study, and its nominal composition is listed in Table 1. The particle size of this powder is 15–45 μm , and the powder exhibited a nearly spherical particle shape, as shown in Fig. 1. Q235 low-carbon steel with dimensions of 40 mm \times 40 mm \times 3 mm served as the substrate. The substrate was previously machined, degreased in acetone, dried in air and sandblasted prior to spraying by a Tafa-JP8000 spray system. The spraying distance was 280 mm, the flow rate of oxygen was 967 L/min, the flow rate of kerosene was 0.47 L/min, the powder feed rate was fixed at 5 rpm, and the traverse velocity of the spray gun was 600 mm/s. During and after spraying, the substrates were cooled with compressed air jets. The conventional EHC coating (Xiang Teng Ying Luo Industrial Technology) was deposited using a chromic acid solution with 250 g/L of CrO_3 and 2.5 g/L of H_2SO_4 , a deposition temperature of 50–55 $^\circ\text{C}$, a current density ranging from 0.31 to 0.46 A/dm² and a deposition rate of 25 $\mu\text{m}/\text{h}$.

2.2 Testing Methods

The microstructure of the Fe-based alloy coating was observed in a scanning electron microscope (SEM, Hitachi S-3400N, Japan). The phase compositions of the powder and the coating were investigated by x-ray diffraction (XRD, Bruker D8-Advanced, Germany) with CuK_α radiation. Selected area electron diffraction (SEAD) and finer-scale microstructure characterization of the coating were performed using a transmission electron microscope (TEM, JEOL-2100F, Japan) operated at 200 kV. Porosity measurements were taken from polished cross sections of the coating at a magnification of 500 \times using an optical microscope (OM, Olympus BX51M, Japan) fitted with a DT-2000 image analyzer using the grayscale method. Fifteen images were selected for each average value. Each image was selected randomly, and the porosity was calculated from the proportion of the area of the black zones in the images (pores) and the area of whole image.

An EG&G Princeton Applied Research Model PARASTAT 2273 electrochemical system was used to evaluate the corrosion behavior of the Fe-based coating and the EHC coating in various corrosion environments. The specimens were sealed with a mixture of colophony and paraffin with a geometric area of only 1 cm² exposed to the solution. It should be noted that the real exposed area is related to the defects of the coating, the surface roughness and the electrolyte penetration (Ref 18, 19). Prior to

the electrochemical measurements, the free surfaces of the samples were sequentially ground with 240–1500 mesh grade SiC abrasive papers, then degreased with acetone and dried in air. A conventional three-electrode system was used to perform the electrochemical measurements, with a Pt wire as the counter electrode, a $\text{Hg}|\text{Hg}_2\text{Cl}_2|\text{KCl}$ (Saturated) system as the reference electrode, and the specimen as the working electrode. Experiments were carried out in a 3.5% NaCl solution, a 1 mol/L HCl solution and a 1 mol/L NaOH solution at room temperature (25 $^\circ\text{C}$). The specimens were immersed for 1 h to stabilize the open-circuit potential before conducting the experiment. The potentiodynamic polarization was swept from -0.25 to $+1.6 V_{\text{SCE}}$ relative to the open-circuit potential at a fixed rate of 1 mV/s. Electrochemical impedance spectroscopy (EIS) measurements were taken using a sinusoidal potential perturbation of 10 mV in a frequency range from 10 mHz to 100 kHz. Three specimens were tested for each system to ensure good reproducibility. After electrochemical measurement, the corrosion morphologies of the Fe-based coatings were observed by SEM (Zeiss Gemini Sigma 300, Germany), and the corrosion products were analyzed using energy-disperse spectroscopy (EDS, Bruker XFlash 6160, Germany).

3. Results and Discussion

3.1 Microstructural Characterization

The SEM image in Fig. 2 illustrates the typical morphology in the cross section of the Fe-based coating. The thickness of the coating is approximately 200 μm (Fig. 2(a)). It is obvious that this coating has a dense and homogenous microstructure, and it is well bonded to the substrate, which is in agreement with the results observed in previous investigations of other HVOF-sprayed coatings (Ref 20, 21). In addition, a few unmelted or partially melted particles are visible in this coating (Fig. 2(b)), and several micropores can be observed within the splats or along the interface of two adjacent layered splats. The

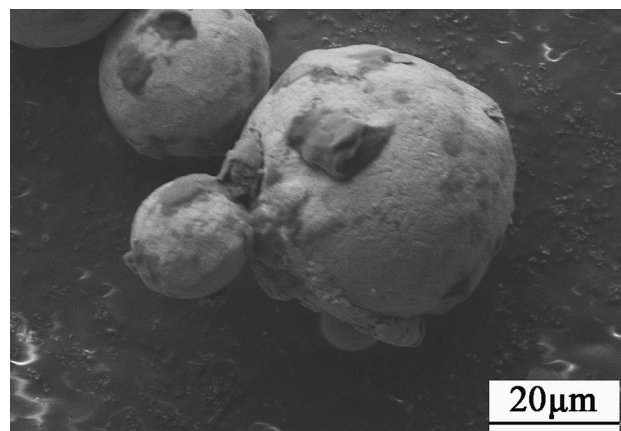


Fig. 1 SEM morphology of the Fe-based powder

Table 1 Nominal composition of the commercial Fe-based alloy powder

Composition	Cr	Ni	Co	Mo	B	Cu	Si	C	S	Fe
Mass percent	28.0–32.0	17.0–21.5	8.4–11.0	3.3–4.5	3.1–4.0	2.0–4.0	1.0–1.6	≤ 0.12	≤ 0.02	Bal.

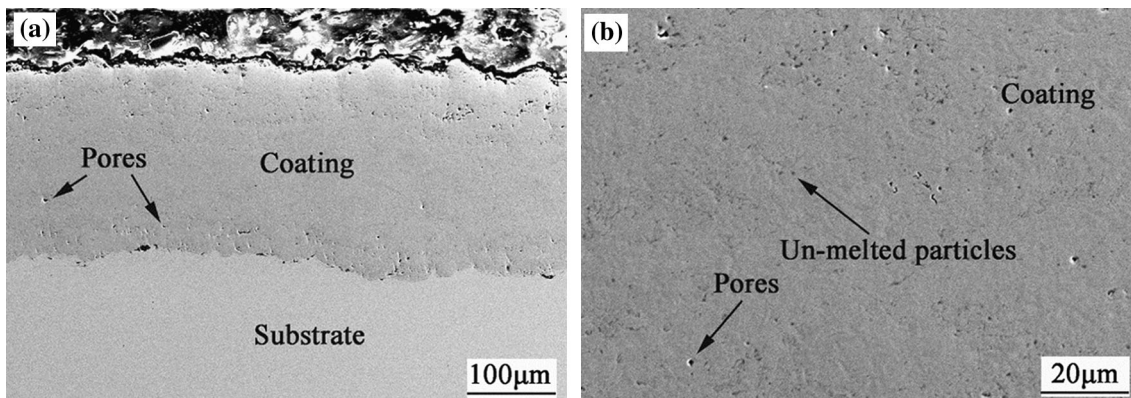


Fig. 2 SEM cross-sectional morphology of the Fe-based coating: (a) low magnification; (b) high magnification

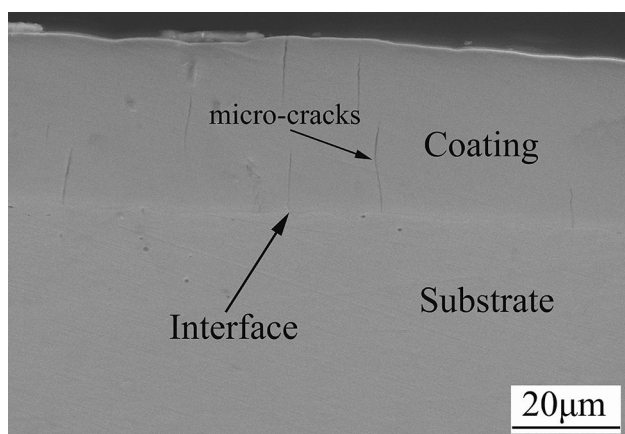


Fig. 3 SEM cross-sectional morphology of the EHC coating

porosity of this coating was calculated to be $0.48\% \pm 0.15\%$. In general, the small pores within the flattened particles were mainly caused by shrinkage, while the large pores located between lamellae were considered to be caused by the gas porosity phenomenon (Ref 22). The microstructure of the EHC coating is shown in Fig. 3. The EHC coating has a thickness of approximately $20\ \mu\text{m}$, which is the typical thickness of the chrome plating on engineering components. In addition, some typical micro-cracks across the EHC coating are seen in the image.

3.2 XRD and TEM Analysis

The x-ray diffraction patterns of the feed powder and the as-sprayed coating are shown in Fig. 4. The XRD patterns indicate the presence of the α -Fe (Cr) solid solution, along with certain amounts of CrB, Cr_2B , FeB, Fe_2B and Ni_2B . Compared to the XRD pattern of the powder, the diffraction peaks of the coating are weaker and broader. Furthermore, the strongest diffraction peak of the coating at a 2θ of approximately 45° is quite broad, so it can be deduced that a partially amorphous phase exists in the Fe-based coating. Similar results were shown in other studies (Ref 23, 24). The fraction of the amorphous phase was calculated to be 48.23% by the Verdon method (Ref 25). In addition, no peaks characteristic of any oxides were observed in the XRD pattern of the coating due to the advantages of the HVOF spraying technology (Ref 12). A low oxide content is

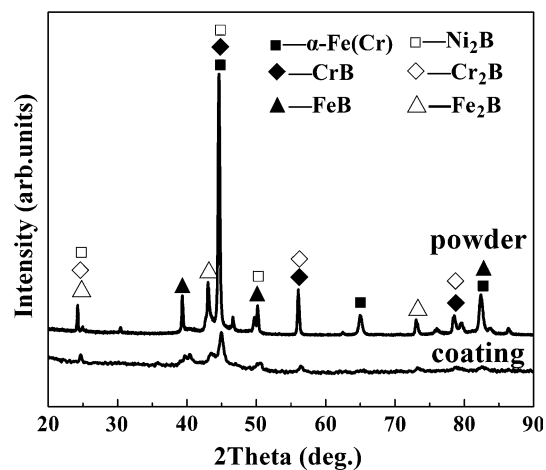


Fig. 4 X-ray diffraction patterns of the feed powder and the Fe-based coating

conductive to forming an amorphous phase and improving the quality of the coating (Ref 26).

To provide more detailed information, the microstructure of the as-sprayed coating was studied using TEM, as shown in Fig. 5. This revealed that a portion of the microstructure of the coating consists of nanocrystalline grains embedded in a matrix largely composed of amorphous phase. The diffused halo ring in the SEAD pattern (inset of Fig. 5) confirms the existence of the amorphous phase, and nanocrystalline grains can be clearly seen in the image.

3.3 Electrochemical Corrosion Behavior

3.3.1 Potentiodynamic Polarization Curves. Figure 6 shows the potentiodynamic polarization curves of the Fe-based coating and the EHC coating in a 3.5% NaCl solution (a), a 1 mol/L HCl solution (b) and a 1 mol/L NaOH (c) solution, respectively. It is obvious that the Fe-based coating and the EHC coating both experienced active dissolution, passivation and transpassivation processes. In the 3.5% NaCl solution, the Fe-based coating and the EHC coating both exhibit a spontaneous passivation with a similar passive region of approximately 600 mV, but the passive current density of the former is two orders of magnitude smaller than that of the latter. In the 1 mol/L HCl and NaOH solutions, the Fe-based coating has a

spontaneous passivation with a much wider passive region and a lower passive current density than the EHC coating. These results demonstrate that the Fe-based coating has a superior passive film protection ability compared to the EHC coating in the aforementioned solutions. For the Fe-based coating, its transpassive potential is approximately 1.0 V in the three solutions, indicating good resistance to localized corrosion.

Table 2 lists the calculated values of the corrosion potential (E_{corr}) and the corrosion current density (i_{corr}) based on the Tafel extrapolation (Ref 27). As listed in Table 2, the corrosion potential of the Fe-based coating is -196 mV in the 3.5% NaCl solution, much higher than the -554 mV corrosion potential of the EHC coating. In addition, the corrosion current density of the Fe-based coating is $0.14 \mu\text{A}/\text{cm}^2$, much lower than the $14.12 \mu\text{A}/\text{cm}^2$ corrosion current density of the EHC coating. It is generally accepted that a higher corrosion potential represents a higher chemical stability and a lower corrosion tendency, while a lower corrosion current density indicates a lower corrosion rate (Ref 28). Therefore, the Fe-based coating has a lower tendency to corrode and a better corrosion resistance in a 3.5% NaCl solution than the EHC coating.

In the 1 mol/L HCl solution, the corrosion potential of the Fe-based coating is -383 mV, higher than the potential of the EHC coating by 151 mV, which means that the corrosion tendency of the Fe-based coating is smaller than that of the EHC coating. Simultaneously, the corrosion current density of the EHC coating is $709.2 \mu\text{A}/\text{cm}^2$, much larger than that of the Fe-based coating, indicating that the corrosion resistance of the

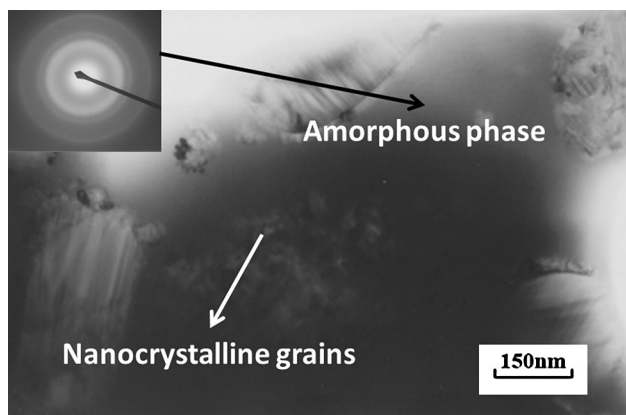


Fig. 5 TEM image of a typical microstructure of the Fe-based coating

Fe-based coating is better than the resistance of the EHC coating in 1 mol/L HCl solution.

In 1 mol/L NaOH solution, the corrosion potential of the Fe-based coating is only 26 mV larger than that of the EHC coating, while the corrosion current density of the Fe-based coating is approximately 10 times that of the EHC coating. Therefore, it can be concluded that the corrosion resistance of the Fe-based coating is inferior to the corrosion resistance of the EHC coating in the 1 mol/L NaOH solution.

3.3.2 EIS Plots of the Coatings. EIS tests were also performed to study the corrosion behavior of the Fe-based coating and the EHC coating in various solutions. Figure 7 shows the Nyquist plots for the Fe-based coating and the EHC coating in a 3.5% NaCl solution (a), a 1 mol/L HCl solution (b) and a 1 mol/L NaOH (c) solution at open-circuit potential (OCP), respectively.

In the 3.5% NaCl solution, both EIS curves present only one capacitive loop (Fig. 7(a)), which means that both coatings have only one time constant. In addition, the diameter of the capacitance arc for the EHC coating is smaller, indicating that the EHC coating exhibits less corrosion resistance than the Fe-based coating. Because of the spontaneous passivation of the Fe-based coating and the formation of a dense passive film in the NaCl solution, the R(QR) equivalent circuit (Fig. 8(a)) was employed to model the EIS plots of the coating (Ref 29). A constant phase element (CPE) is commonly used to replace capacitance, because a real electrochemical process rarely has a pure capacitance. CPE is an element used in place of a capacitor to compensate for non-homogeneity in the system. CPE is characterized by two parameters (Q and n), Q represents the admittance constant (dielectric behavior or capacity) and n is an empirical exponent of the CPE, which is between 0 and 1. In fact, the CPE can be considered as a non-ideal capacitor and for an ideal capacitance n is equal to 1 (Ref 30). The equivalent circuit for Fig. 8(a) consists of the resistance of the solution (R_s), the resistance of the coating (R_c) and the capacitance of the coating (Q_c). The fitting parameters of the Fe-based coating and the EHC coating are listed in Table 3. The resistance of the Fe-based coating in the 3.5% NaCl solution is $2.26 \times 10^6 \Omega \text{ cm}^2$, which is 1000 times higher than the resistance of the EHC coating. All of the results indicate that the corrosion resistance of the Fe-based coating is better than that of the EHC coating in the 3.5% NaCl solution.

Figure 7(b) shows the Nyquist plot of the Fe-based coating and the EHC coating in the 1 mol/L HCl solution. The curves for the Fe-based coating and the EHC coating both present two capacitive loops, one appearing in the low-frequency region

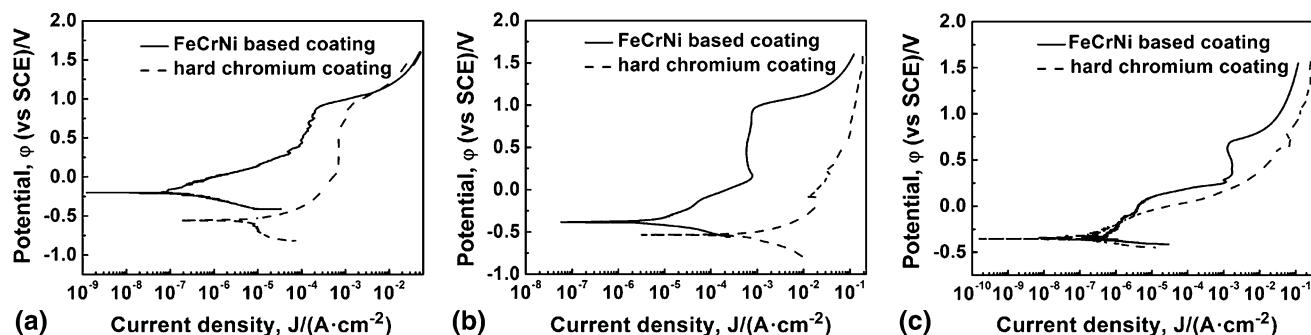


Fig. 6 Potentiodynamic polarization curves of samples in various solutions: (a) 3.5% NaCl solution; (b) 1 mol/L HCl solution; (c) 1 mol/L NaOH solution

Table 2 Summary of the electrochemical parameters of the samples from the potentiodynamic polarization curves

Corrosive solutions	E_{corr} mV		i_{corr} $\mu\text{A}/\text{cm}^2$	
	FeCrNi-based coating	Hard chromium coating	FeCrNi-based coating	Hard chromium coating
3.5% NaCl	-196	-554	0.14	14.12
1 mol/L HCl	-383	-534	15.0	709.2
1 mol/L NaOH	-323	-349	0.98	0.11

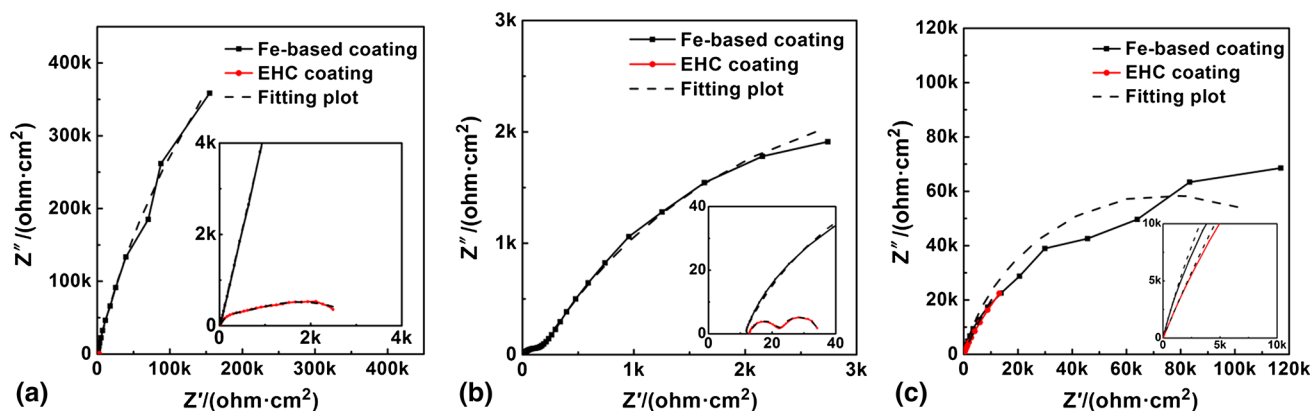


Fig. 7 Nyquist plots of the Fe-based coating and the EHC coating in various solutions: (a) 3.5% NaCl solution; (b) 1 mol/L HCl solution; (c) 1 mol/L NaOH solution

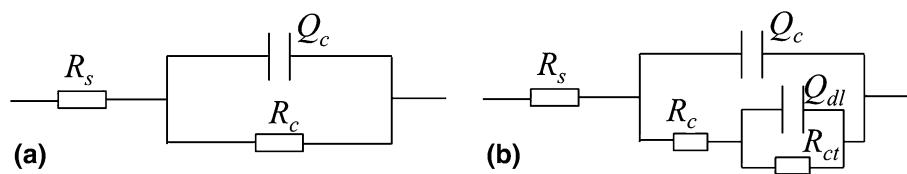


Fig. 8 Equivalent circuit representative of the Fe-based coating and the EHC coating: (a) in 3.5% NaCl solution and 1 mol/L NaOH solution; (b) in 1 mol/L HCl solution

Table 3 Electrochemical parameters obtained from EIS of the Fe-based coating and the EHC coating in various solutions

Medium	Coating	R_s , $\Omega \text{ cm}^2$	Q_c , $\mu\text{m}/\text{cm}^2$	n_c	R_c , $\Omega \text{ cm}^2$	Q_{dl} , $\mu\text{m}/\text{cm}^2$	n_{dl}	R_{ct} , $\Omega \text{ cm}^2$
3.5% NaCl	FeCrNi	12.19	27.06	0.860	2.26×10^6
	Cr	12.74	93.28	0.658	2.04×10^3
1 mol/L HCl	FeCrNi	12.92	70.9	0.736	6959	1321	0.625	283.2
	Cr	13.04	234.5	0.898	13	32,800	0.867	9.267
1 mol/L NaOH	FeCrNi	11.61	44.0	0.845	1.50×10^5
	Cr	10.64	313.4	0.756	2.63×10^5

and other in the high-frequency region, indicating that there are two time constants. Generally, the high-frequency loop is physically related to the coating defects, while the low-frequency loop is related to the corrosion process (Ref 31). It is obvious that both of the capacitive loops of the Fe-based coating are bigger than the loops for the EHC coating, suggesting that the EHC coating is easier for the solution to penetrate through due to its inherent micro-cracks and that local corrosion is easier to generate at the coating/substrate interface. Based on the above analysis, a $R(Q(R(QR)))$ equivalent circuit was adopted (Fig. 8(b)). Q_{dl} represents the capacitance of the double layer, and R_{ct} represents the charge transfer resistance at the coating/substrate interface. As listed in Table 3, the R_c ($6539 \Omega \text{ cm}^2$) and R_{ct} ($283.2 \Omega \text{ cm}^2$) of the Fe-based coating in

the 1 mol/L HCl solution are much higher than the R_c ($13 \Omega \text{ cm}^2$) and R_{ct} ($9.267 \Omega \text{ cm}^2$) of the EHC coating. Based on the analysis above, the Fe-based coating shows better corrosion resistance than the EHC coating in a 1 mol/L HCl solution.

Figure 7(c) shows the Nyquist plot of the Fe-based coating and the EHC coating in the 1 mol/L NaOH solution. Both curves have a single capacitive loop, so the equivalent circuit illustrated in Fig. 8(a) was adopted to study the corrosion behavior of the Fe-based coating and the EHC coating in the 1 mol/L NaOH solution. The loop of the EHC coating has a larger diameter than the loop of the Fe-based coating, which means that the Fe-based coating has less corrosion resistance than the EHC coating in a 1 mol/L NaOH solution. As listed in Table 3, the R_c of the EHC coating is $2.63 \times 10^5 \Omega \text{ cm}^2$, higher

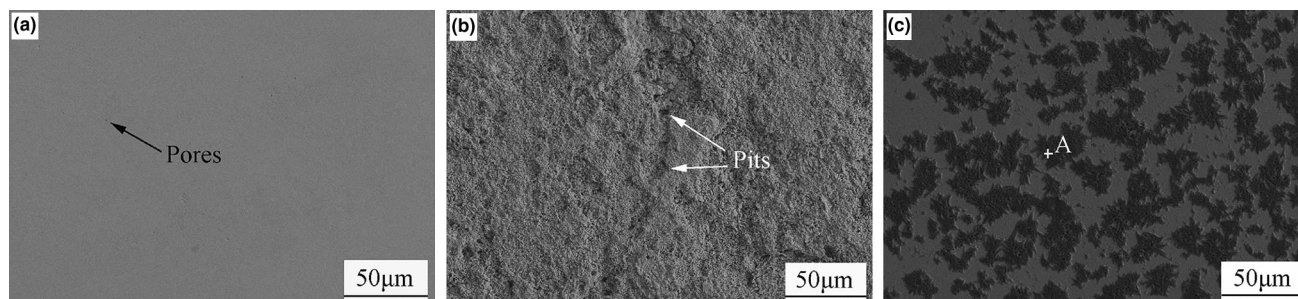


Fig. 9 SEM images of the surfaces of Fe-based coatings after electrochemical measurements in: (a) 3.5% NaCl solution, (b) 1 mol/L HCl solution and (c) 1 mol/L NaOH solution

Table 4 Composition of the corrosion products of the Fe-based coating in 1 mol/L NaOH solution

Composition	Cr K	Fe K	O K	Na K	B K	Cu K	Si K	C K	Ni K	Co K
Atom percent	33.17	20.52	18.60	12.70	3.91	0.29	2.95	7.16	0.25	0.45

than the $1.50 \times 10^5 \Omega \text{ cm}^2$ resistivity of the Fe-based coating, providing further evidence that the Fe-based coating has an inferior corrosion resistance compared to the EHC coating in a 1 mol/L NaOH solution.

In 3.5% NaCl solution and in 1 mol/L HCl solution, the Fe-based coating shows better corrosion resistance than the EHC coating, which could be attributed to the dense structure and fewer defects of the Fe-based coating. These advantages can prevent the chloride ions from penetrating into the coating easily. However, the Fe-based coating has less corrosion resistance than the EHC coating in the 1 mol/L NaOH solution. This is because the EHC coating has an inherently great corrosion resistance in alkaline solution (Ref 32). Initially, the corrosive liquid can attack the EHC coating through pores and micro-cracks to easily form a hydroxide film and destroy the coating. This hydroxide film has a very dense structure and can isolate the coating from the corrosive liquid, thus retarding any further corrosion of the EHC coating.

Moreover, it is found that the Fe-based coating has a better corrosion resistance in the 3.5% NaCl solution than in the 1 mol/L HCl solution. In the 3.5% NaCl solution, on the one hand, chloride ions can react with metal ions in the coating to form soluble compounds that will destroy the passive film. On the other hand, hydroxide ions will combine with the metal cations which will prevent chloride ions from reaching the coating. The passive film thus formed is hard to destroy, and the corrosion resistance is enhanced (Ref 33). However, in the 1 mol/L HCl solution, the high hydrogen ion concentration will lead to a rapid cathodic reaction rate and anodic polarization of the coating (Ref 34); therefore, the Fe-based coating has a lower corrosion resistance in the 1 mol/L HCl solution than in the NaCl solution. In addition, the Fe-based coating also has better corrosion resistance in the 3.5% NaCl solution than in the 1 mol/L NaOH solution. The passive film in the NaOH solution is hydrogen-based oxide, with bonded water, whose structure can be expressed as (-M-H₂O-M-) or (-M-OH-M-). The bound water is considered to be an active site in the passive film, which can make the film unstable (Ref 35). Therefore, too many hydroxide ions will generate too many active points, these less stable points are easy to dissolve and thus the ability

to protect the coating is lost. Therefore, the Fe-based coating has less corrosion resistance in a 1 mol/L NaOH solution than in the 3.5% NaCl solution.

3.3.3 Morphologies of the Corroded Surfaces. To better understand the corrosion behavior of the Fe-based coatings in the various solutions, the coatings after electrochemical measurements were further examined by SEM. The corrosion morphology of the Fe-based coating after electrochemical measurement in the 3.5% NaCl solution, as shown in Fig. 9(a), is similar to its surface morphology before the testing, demonstrating that the Fe-based coating has high corrosion resistance in the 3.5% NaCl solution. Unfortunately, as shown in Fig. 9(b), many tiny pits are observed on the surface of the coating after electrochemical measurement in the 1 mol/L HCl solution, indicating that the Fe-based coating primarily suffered pitting corrosion in the acid solution. This observation agrees with the finding that the Fe-based coating has a poor corrosion resistance in a 1 mol/L HCl solution. Figure 9(c) shows the corrosion morphology of the Fe-based coating after electrochemical measurement in the 1 mol/L NaOH solution. It is apparent that some black corrosion products have formed on the coating. The composition of the corrosion products (point A) was obtained by EDS and is listed in Table 4. The corrosion products contain a high amount of Fe, Cr, O and Na, implying that the corrosion products have the structure of (-M-H₂O-M-) or (-M-OH-M-). The corrosion products are considered to be active sites of the coating (Ref 35), and this is consistent with the above analyses.

4. Conclusions

1. HVOF thermal spraying technology was adopted to prepare the Fe-based coating on Q235 steel. The coating has a dense structure, with a porosity of $0.48\% \pm 0.15\%$. The Fe-based coating was composed of an amorphous phase, nanocrystalline grains and several kinds of borides.
2. The Fe-based coating exhibits better corrosion resistance in a 3.5% NaCl solution and a 1 mol/L HCl solution than

the EHC coating because of the dense structure and fewer defects of the Fe-based coating, while the Fe-based coating shows less corrosion resistance than the EHC coating in a 1 mol/L NaOH solution because of the lower passivation of the Fe-based coating relative to the EHC coating.

3. The Fe-based coating has better corrosion resistance in the 3.5% NaCl solution than in the 1 mol/L HCl solution or the 1 mol/L NaOH solution, which is primarily attributed to the hydrogen ion concentration and the hydroxide ion concentration of the solutions.

Acknowledgments

The research was supported by the National Natural Science Foundation of China (Grant Nos. 51579087, 51609067 and 51301059), the Natural Science Foundation of Jiangsu Province of China (Grant No. BK20150806), the China Postdoctoral Science Foundation (Grant No. 2016M590404), the Opening Project of Material Corrosion and Protection Key Laboratory of Sichuan Province (Grant No. 2016CL08) and the Fundamental Research Funds for the Central Universities (Grant Nos. 2015B01514 and 2016B45714). The authors also gratefully acknowledge the financial support from the CAS Key Laboratory of Nuclear Materials and Safety Assessment, Institute of Metal Research, Chinese Academy of Sciences (Grant No. 2016NMSAKF03).

References

1. R.Q. Guo, C. Zhang, Y. Yang, Y. Peng, and L. Liu, Corrosion and Wear Resistance of a Fe Based Amorphous Coating in Underground Environment, *Intermetallics*, 2012, **30**, p 94
2. A. Milanti, V. Matikainen, H. Koivuluoto, G. Bolelli, L. Lusvardi, and P. Vuoristo, Effect of Spraying Parameters on the Microstructural and Corrosion Properties of HVAF-Sprayed Fe-Cr-Ni-B-C Coatings, *Surf. Coat. Technol.*, 2015, **277**, p 81
3. Z. Zeng, N. Sakoda, T. Tajiri, and S. Kuroda, Structure and Corrosion Behavior of 316L Stainless Steel Coatings Formed by HVAF Spraying With and Without Sealing, *Surf. Coat. Technol.*, 2008, **203**, p 284
4. J.M. Guilemany, N. Espallargas, P.H. Suegama, and A.V. Benedetti, Comparative Study of Cr₃C₂-NiCr Coatings Obtained by HVOF and Hard Chromium Coatings, *Corros. Sci.*, 2006, **48**, p 2998
5. J. Kawakita, T. Fukushima, S. Kuroda, and T. Kodama, Corrosion Behaviour of HVOF Sprayed SUS316L Stainless Steel in Seawater, *Corros. Sci.*, 2002, **44**, p 2561
6. J.F. Flores, A. Neville, N. Kapur, and A. Gnanavelu, Corrosion and Erosion-Corrosion Processes of Metal-Matrix Composites in Slurry Conditions, *J. Mater. Eng. Perform.*, 2012, **21**, p 395
7. B. Xu, M. Shining, and J. Wang, Application of Electric Arc Spraying Technique to Enhance Corrosion Resistance of Steel Structures on Ships, *Surf. Eng.*, 1995, **11**, p 38
8. K. Cooke, G. Oliver, V. Buchanan, and N. Palmer, Optimisation of the Electric Wire Arc-Spraying Process for Improved Wear Resistance of Sugar Mill Roller Shells, *Surf. Coat. Technol.*, 2007, **202**, p 185
9. Y.C. Zhu, K. Yukimura, C.X. Ding, and P.Y. Zhang, Tribological Properties of Nanostructured and Conventional WC-Co Coatings Deposited by Plasma Spraying, *Thin Solid Films*, 2001, **388**, p 277
10. D.A. Stewart, P.H. Shipway, and D.G. McCartney, Abrasive Wear Behaviour of Conventional and Nanocomposite HVOF-Sprayed WC-Co Coatings, *Wear*, 1999, **255**, p 789
11. L. Ajdelsztajn, J.A. Picas, G.E. Kim, F.L. Bastian, J. Schoenung, and V. Probenzano, Oxidation Behavior of HVOF Sprayed Nanocrystalline NiCrAlY Powder, *Mater. Sci. Eng. A Struct.*, 2002, **338**, p 33
12. Y.P. Wu, P.H. Lin, G.Z. Xie, J. Hu, and M. Cao, Formation of Amorphous and Nanocrystalline Phases in High Velocity Oxy-Fuel Thermally Sprayed a Fe-Cr-Si-B-Mn Alloy, *Mater. Sci. Eng. A Struct.*, 2006, **430**, p 24
13. Z. Zhou, L. Wang, F.C. Wang, H.F. Zhang, Y.B. Liu, and S.H. Xu, Formation and Corrosion Behavior of Fe-Based Amorphous Metallic Coatings by HVOF Thermal Spraying, *Surf. Coat. Technol.*, 2009, **204**, p 563
14. C. Zhang, R.Q. Guo, Y. Yang, Y. Wu, and L. Liu, Influence of the Size of Spraying Powders on the Microstructure and Corrosion Resistance of Fe-Based Amorphous Coating, *Electrochim. Acta*, 2011, **56**, p 6380
15. Y. Yang, C. Zhang, Y. Peng, Y. Yu, and L. Liu, Effects of Crystallization on the Corrosion Resistance of Fe-Based Amorphous Coatings, *Corros. Sci.*, 2012, **59**, p 10
16. X.Q. Liu, Y.G. Zheng, X.C. Chang, W.L. Hou, and J.Q. Wang, Influence of HVOF Thermal Spray Process on the Microstructures and Properties of Fe-Based Amorphous/Nano Metallic Coatings, *Mater. Sci. Forum*, 2010, **633**, p 685
17. M.S. Bakare, K.T. Voisey, K. Chokethawai, and D.G. McCartney, Corrosion Behaviour of Crystalline and Amorphous Forms of the Glass Forming Alloy Fe₄₃Cr₁₆Mo₁₆C₁₅B₁₀, *J. Alloy. Compd.*, 2012, **527**, p 210
18. P.H. Suegama, N. Espallargas, J.M. Guilemany, J. Fernández, and A.V. Benedetti, Electrochemical and Structural Characterization of Heat-Treated Cr₃C₂-NiCr Coatings, *J. Electrochem. Soc.*, 2006, **153**, p 434
19. P.H. Suegama, C.S. Fugivara, A.V. Benedetti, J. Fernández, N. Espallargas, J. Delgado, and J.M. Guilemany, Microstructure and Electrochemical Studies of Cr₃C₂-NiCr Coatings, *New Research on Electrochemistry*, chap. 4, E.P. Vargus, Ed., Nova Science Publishers, Inc., New York, 2007, p 206
20. S. Hong, Y.P. Wu, J.F. Zhang, Y. Qin, and J. Lin, Effect of Ultrasonic Cavitation Erosion on Corrosion Behavior of High-Velocity Oxygen-Fuel (HVOF) Sprayed Near-Nanostructured WC-10Co-4Cr Coating, *Ultrason. Sonochem.*, 2015, **27**, p 374
21. Z.B. Zheng, Y.G. Zheng, W.H. Sun, and J.Q. Wang, Effect of Heat Treatment on the Structure, Cavitation Erosion and Erosion-Corrosion Behavior of Fe-Based Amorphous Coatings, *Tribol. Int.*, 2015, **90**, p 393
22. V.V. Sobolev and J.M. Guilemany, Investigation of Coating Porosity Formation During High Velocity Oxy-Fuel (HVOF) Spraying, *Mater. Lett.*, 1994, **18**, p 304
23. Y.P. Wu, P.H. Lin, Z. Wang, and G. Li, Microstructure and Microhardness Characterization of a Fe-Based Coating Deposited by High-Velocity Oxy-Fuel Thermal Spraying, *J. Alloy. Compd.*, 2009, **481**, p 719
24. J. Farmer, J.S. Choi, C. Saw, J. Haslam, D. Day, P. Hailey, and D. Branagan, Iron-Based Amorphous Metals: High-Performance Corrosion-Resistant Material Development, *Metall. Mater. Trans. A*, 2009, **40**, p 1289
25. M.L. Gualtieri, M. Prudenziati, and A.F. Gualtieri, Quantitative Determination of the Amorphous Phase in Plasma Sprayed Alumina Coatings Using the Rietveld Method, *Surf. Coat. Technol.*, 2006, **201**, p 2984
26. Y. Wang, Z.Z. Xing, Q. Luo, A. Rahman, J. Jiao, S.J. Qu, and J. Shen, Corrosion and Erosion-Corrosion Behaviour of Activated Combustion High-Velocity Air Fuel Sprayed Fe-Based Amorphous Coatings in Chloride-Containing Solutions, *Corros. Sci.*, 2015, **98**, p 339
27. Standard, A. S. T. M., G59-97, *Standard Test Method for Conducting Potentiodynamic Polarization Resistance Measurements*, ASTM International, West Conshohocken, 2009
28. R.F. Li, Z.G. Li, Y.Y. Zhu, and K. Qi, Structure and Corrosion Resistance Properties of Ni-Fe-B-Si-Nb Amorphous Composite Coatings Fabricated by Laser Processing, *J. Alloy. Compd.*, 2013, **580**, p 327
29. J.M. Guilemany, J. Fernández, N. Espallargas, P.H. Suegama, and A.V. Benedetti, Influence of Spraying Parameters on the Electrochemical Behaviour of HVOF Thermally Sprayed Stainless Steel Coating in 3.4% NaCl, *Surf. Coat. Technol.*, 2006, **200**, p 3064
30. M.M. Verdian, K. Raeissi, and M. Salehi, Fabrication and Corrosion Resistance of HVOF-Sprayed Ni₂Si Intermetallic Compound, *Appl. Surf. Sci.*, 2013, **273**, p 426
31. Z. Yao, Z. Jiang, S. Xin, X. Sun, and X. Wu, Electrochemical Impedance Spectroscopy of Ceramic Coatings on Ti-6Al-4V by Micro-plasma Oxidation, *Electrochim. Acta*, 2005, **50**, p 3273
32. D. Toma, W. Brandl, and G. Marginean, Wear and Corrosion Behaviour of Thermally Sprayed Cermet Coatings, *Surf. Coat. Technol.*, 2001, **138**, p 149
33. D. Zhu and W.J. van Ooij, Corrosion Protection of AA 2024-T3 by Bis-[3-(Triethoxysilyl) Propyl] Tetrasulfide in Sodium Chloride Solution: Part 2: Mechanism for Corrosion Protection, *Corros. Sci.*, 2003, **45**, p 2177

34. J.G. Yu, J.L. Luo, and P.R. Norton, Electrochemical Investigation of the Effects of Hydrogen on the Stability of the Passive Film on Iron, *Electrochim. Acta*, 2002, **47**, p 1527
35. G. Okamoto and T. Shibata, Stability of Passive Stainless Steel in Relation to the Potential of Passivation Treatment, *Corros. Sci.*, 1970, **10**, p 371